Environmental Science Nano

Uptake and depuration of carbon- and boron nitride-based nanomaterials in the protozoa Tetrahymena thermophila

Journal:	*Environmental Science: Nano*
Manuscript ID	EN-ART-08-2021-000750.R1
Article Type:	Paper

Environmental significance statement

Bioaccumulation is an important component of risk assessment of environmental pollutants; however, conventional methods are inadequate for quantification of uptake and depuration kinetics of carbon-based engineered nanomaterials (ENMs). This study proposes a rapid and accurate microscopy-based method for bioaccumulation quantification of insoluble ENMs, using a single-celled freshwater organism, ciliated protozoa and a one-compartment kinetic modeling approach. The method is extendable to other insoluble particulate nano- or micromaterials, such as plastics, whose bioaccumulation is driven by physical and dynamic processes. The results of the study indicate longer residence times of high-aspect-ratio ENMs in the protozoan food vacuoles which may pose environmental and human health risks, and warrants similar investigations of microfibers, the most prevalent type of microplastics in the environment.

ARTICLE

Uptake and Depuration of Carbon- and Boron Nitride-Based Nanomaterials in the Protozoa *Tetrahymena thermophila*

Monika Mortimer, [a, b, c] Timnit Kefela, [b, c] Anne Trinh [b] and Patricia A. Holden * [b, c]

Received 00th January 20xx,
Accepted 00th January 20xx

DOI: 10.1039/x0xx00000x

Quantifying bioaccumulation is important in environmental contaminant risk assessment. Engineered nanomaterials (ENMs) are contaminants of emerging concern (CECs) that can enter organisms and bioaccumulate, but more understanding is needed regarding how to measure and model ENM biological uptake and elimination. Conventional chemical analysis and microscopic approaches inadequately differentiate ENMs from carbon-rich organisms, and thus do not allow for directly understanding where, and to what degree, ENMs bioaccumulate in organisms. Here we present a microscopy and image analysis-based approach for quantifying uptake and depuration kinetics of carbonaceous ENMs; we also apply the methods to boron nitride-based ENMs. The phagotrophic protist *Tetrahymena thermophila* was exposed to subinhibitory levels (10 mg L^{-1}) of multiwall carbon nanotubes (CNTs), graphene nanoplatelets (GNPs), carbon black (CB), hexagonal boron nitride flakes (hBN) and boron nitride nanotubes (BNNTs). Uptake and depuration were assessed using quantitative microscopy of ENMs in food vacuoles, with the results for CNTs benchmarked to prior studies using ^{14}C-labeled ENMs. Kinetically derived bioaccumulation factors (BCFs) indicated that only hBN was bioaccumulative, i.e. with a BCF > 1000 L kg^{-1}. The uptake rates were similar for all three carbonaceous ENMs, but significantly higher and lower, respectively, for hBN and BNNTs compared to carbonaceous ENMs. Uptake appeared to correlate with the tapped densities of the ENMs, i.e., ratio of ENM mass to the volume occupied after tapping to constant volume, assumed to be representative of the ENM "packing" density in protozoan food vacuoles. Depuration was relatively slower for the tubular ENMs (CNTs and BNNTs) compared to planar (GNPs and hBN) and spherical (CB) ENMs, and the first order depuration rate coefficients measured over 2 hours correlated significantly (P=0.03) with ENM aspect ratios (the ratio of length to width of a particle) which were highest for the tubular ENMs. This suggests that intracellular residence times are longer for high-aspect-ratio ENMs due to impaired phagosomal expulsion. Such findings, and the approaches herein, may be relevant when considering bioaccumulation of other C-rich CECs such as nano- or micro-plastic particles or fibers, for which crucial environmental risk assessment data are limited.

1. Introduction

In efforts to provide solutions to global challenges like clean water access and energy storage, technologies centered on the use of engineered nanomaterials (ENMs) which vary in chemistry, morphology and reactivity are sought after.[1] Among ENMs, carbon-based materials constitute a major category which have high production volumes worldwide, are being incorporated into a wide range of products, and consequently pose an elevated risk for environmental release and exposures.[2, 3] Boron nitride (BN)-based ENMs have emerged more recently as alternatives for carbon-based ENMs, with advantageous properties. Thus, their use will likely increase in the future,[4] potentially resulting in increased environmental exposures.

An important part of risk assessment of chemicals is an evaluation of their bioaccumulation potential which is of especially high concern in the case of persistent materials such as carbonaceous ENMs. Further, both carbon- and BN-based ENM families include morphologically distinct materials such as planar (graphene and hexagonal BN flakes), tubular (carbon nanotubes or CNTs and boron nitride nanotubes or BNNTs) and spherical (carbon black) ENMs for which shape-dependent effects and interactions with microorganisms have been demonstrated.[5, 6] This highlights the importance of understanding how ENM shape influences the uptake and elimination of ENMs which determines their bioaccumulation and biomagnification risk. Comparative assessment of bioaccumulation of differently shaped ENMs in invertebrate organisms has been conducted with CuO ENMs (rods, spheres and platelets) and indicated either shape-dependent or -non-dependent uptake and depuration of the ENMs in different species.[7-9] The reason for variable results may be the chemical transformations and speciation of CuO in the organisms which may have affected the uptake, distribution and elimination of the ENMs and complicated the bioaccumulation profile.[10] Carbon- and BN-based ENMs are expected to biotransform in organisms to a lesser extent than soluble metal-based ENMs; still ENM accumulation modeling is a highly debated issue since the models created for conventional solutes are

[a] *Institute of Environmental and Health Sciences, College of Quality and Safety Engineering, China Jiliang University, Hangzhou, Zhejiang 310018, China*
[b] *Bren School of Environmental Science and Management and Earth Research Institute, University of California, Santa Barbara, California 93106, USA*
[c] *University of California Center for the Environmental Implications of Nanotechnology (UC CEIN), University of California, Santa Barbara, California 93106, United States, E-mail: holden@bren.ucsb.edu*
† Footnotes relating to the title and/or authors should appear here.
Electronic Supplementary Information (ESI) available: [details of any supplementary information available should be included here]. See DOI: 10.1039/x0xx00000x

not applicable for ENMs.[11] Biodynamic models which are based on kinetic exposure experiments have been deemed most suitable for quantifying ENM bioaccumulation because these do not assume equilibrium between the organism and exposure medium.[10] The accuracy of the applied model relies largely on the knowledge about the relevant physiological processes driving ENM uptake kinetics and extent, such as the underlying uptake mechanism, ENM distribution, and transformations in the organism. Thus, conducting ENM bioaccumulation studies with organisms that have simple and well-characterized physiology may provide a good model system for the initial screening of ENM bioaccumulation potential.

In addition to the uncertainties in the modeling of ENM bioaccumulation, there are challenges in the quantification of ENMs in biological matrices.[12] Commonly employed quantification methods for carbonaceous ENMs in cells and organisms, which include spectroscopic (absorbance or Raman)[13, 14] and spectrometric (quantification of metal impurities)[15] methods, almost exclusively require ENM extraction from the biological matrix prior to quantitative measurements or are time and energy-intensive.[16, 17] Radiolabeling methods can provide low detection limits, but the experiments require specialized equipment, and generate radioactive waste.[18, 19] Semi-quantitative approaches of CNT cellular uptake include sodium dodecyl sulfate-polyacrylamide gel electrophoresis (SDS-PAGE) of the homogenized cellular sample and integrated optical densitometry of the CNT band in the gel image.[20] However, such approaches do not review intracellular ENM compartmentalization. ENM quantification at the single-cell level, including in environmentally relevant organisms, is afforded by recently reported analytical methods such as single-cell inductively coupled plasma mass spectrometry (SC-ICP-MS) employed with freshwater flagellated microalgae[21] and high-throughput mass cytometry used to detect low levels of Au nanoparticles (NPs) in single cells of the ciliate *Tetrahymena thermophila*.[22] While both methods enable detection of attogram (10^{-18} g) levels of ENMs in single cells, they are not applicable for non-metal ENMs and also do not reveal intracellular distribution.

Owing to their unusual optical and electronic properties, various microscopic techniques have been used for imaging carbonaceous ENMs in cells; these include label-free imaging with transient absorption microscopy,[23] hyperspectral imaging,[24] scanning and transmission electron microscopy (SEM and TEM)[25] and confocal laser scanning microscopy (CLSM) of fluorescently labeled graphene.[26] However, none of these approaches are typically employed quantitatively. Because of the suitable cell size (tens of micrometers) and transparency to optical light, optical microscopy has been successfully used for the characterization of intracellular ENMs in the ciliated protozoan *T. thermophila*. The techniques include hyperspectral imaging[27] and hyperspectral stimulated Raman scattering (SRS) microscopy,[28] but these have neither been used quantitatively nor for carbon-based ENMs. A quantitative study for determining TiO_2 NP masses internalized into *T. thermophila* food vacuoles has been previously conducted using electron microscopy (EM)-based quantitative image analysis.[29] However, since EM requires extensive sample preparation and operation time, the method's throughput for quantitative image analysis is not high.

Here, by taking advantage of the size and physiological properties of the ciliated protozoan *T. thermophila*, an optical microscopy and image analysis-based approach was developed to quantify ENM uptake and depuration, providing data for modeling the process kinetics. The approach allowed for facile and fast sample preparation and higher throughput in terms of the number of captured images compared to EM. The quantitative method was validated based on a prior study where a strong correlation was established between the analytical quantification of ^{14}C-labeled CNTs internalized by *T. thermophila* and comparative semiquantification of unlabeled CNTs by micrograph image analysis.[18] In this study, we developed a quantitative image analysis-based method to assess how the ENM material and aspect ratio affect their uptake and depuration. Thus, we determined the uptake and depuration kinetics of two carbonaceous ENMs (multiwall carbon nanotubes, CNTs, and graphene nanoplatelets, GNPs) and two BN-based ENMs (BNNTs and hexagonal boron nitride flakes, hBN) of different shapes. The ENMs were studied in parallel with carbon black (CB), a non-toxic and non-bioaccumulative industrial carbon nanomaterial.[30] This study employed the environmentally relevant model of *T. thermophila*, a eukaryotic microbe which simultaneously represents a single cell that is also an independently functioning organism. Additionally, the ciliate *T. thermophila* feeds by active phagocytosis, which is similar to the filter-feeding performed by common invertebrate model organisms such as crustaceans and bivalves all of which have similar mechanisms of particulate matter uptake. Finally, the study has broader implications for risk assessment of other fibrous-shaped micro- or nanoparticles such as plastics and fibers, considered emerging contaminants in the environment.

2. Materials and methods

2.1. Nanomaterials

GNPs and CNTs were purchased from Cheap Tubes, Inc. (Grafton, VT), CB (Printex 30) from Dorsett & Jackson Inc. (Los Angeles, CA), and hBN and BNNT from Sigma-Aldrich Inc. (Milwaukee, WI) as powders. ENM stock dispersions were prepared by probe sonication in 400 mg L^{-1} of alginic acid (Sigma-Aldrich, St. Louis, MO) in Nanopure water (Thermo Scientific Barnstead, Waltham, MA) as described elsewhere.[31] Alginic acid noncovalently coated the ENMs, enabling stable aqueous dispersion of the hydrophobic ENMs. ENM hydrodynamic sizes and zeta potentials were measured in Nanopure water and Dryl's medium (the exposure medium in the ENM uptake and depuration experiments)[18] using a Zetasizer Nano ZS-90 (Malvern Instruments, Table 1). Detailed physicochemical characterization of the alginic acid-dispersed ENMs has been reported previously.[31]

2.2. Cultivation of *T. thermophila*

T. thermophila SB210E culture was axenically maintained by passaging every 3 weeks in 2 % proteose peptone broth at room temperature.[18] For experiments, 10 mL of proteose peptone-based growth media (SSP, 1 % proteose peptone, 0.1 % yeast extract, 0.2 % dextrose, 0.003 % Fe-EDTA, all % w/v) in sterile polystyrene Petri plates (10 cm by 15 mm) were inoculated with 100 µL of the protozoan stock culture for growth in a stationary humidity chamber at 30 °C for 17 h.[18, 29, 32] At the mid to late exponential phase, as determined by cell counting using a Neubauer chamber, as described below, the cultures were centrifuged at 1000×g, 5-10 °C for 10

minutes. The cell pellets were suspended in 10 mL of starvation medium (Dryl's medium: 2 mmol L^{-1} sodium citrate, 1 mmol L^{-1} NaH_2PO_4, 1 mmol L^{-1} Na_2HPO_4, 1.5 mmol L^{-1} $CaCl_2$, pH 7.4)[18] and centrifuged at 1000×g, 5-10 °C for 10 minutes. The pellets were resuspended in 10 mL of Dryl's medium and transferred into clean Petri plates for overnight starvation in a humidity chamber at 30 °C. The starved *T. thermophila* cells were centrifuged, washed once in Dryl's medium as above, and resuspended in Dryl's medium. The cell concentration was adjusted to 10^5 cells mL^{-1}.

2.3. Exposure of *T. thermophila* to ENMs

Stock dispersions of alginic acid-dispersed ENMs (200 mg L^{-1}) in Nanopure water were first diluted in 2× Dryl's medium in the ratio of 1 : 1 and then further diluted to 20 mg L^{-1} in Dryl's medium. One mL of each ENM dispersion (20 mg L^{-1}) was pipetted into clear non-treated 12-well polystyrene plates (Thermo Scientific™ Nunc™, Roskilde, Denmark) in two replicates, followed by 1 mL of *T. thermophila* suspension in each well, yielding the final ENM concentration of 10 mg L^{-1} and cell concentration of ~5×10^4 cells mL^{-1}. Dryl's medium was used in place of the ENM dispersion for the control. The plates were incubated in a humidity chamber at 30 °C.

2.4. Cell counting

T. thermophila cells were counted using a Neubauer chamber and optical microscope. Cell samples were fixed with glutaraldehyde (2.5 % by volume) and stored at 4 °C until counting (less than 48 h). Duplicate counts were averaged for each fixed sample of at least three biological replicates.

2.5. Cell viability assay

T. thermophila viability after exposure to ENMs for 1 h as described above was determined by measuring the ATP content, as reported elsewhere.[33] Briefly, ATP was extracted from the protozoan samples with an equal volume of ice-cold 4 % trichloroacetic acid (TCA) in 4 mmol L^{-1} ethylenediaminetetraacetic acid (EDTA) disodium salt dihydrate and samples were stored at -20 °C until analysis. For ATP analysis, 100 µL of Tris–EDTA buffer (0.1 mol L^{-1} Tris and 2 mmol L^{-1} EDTA, adjusted to pH 7.75 with acetic acid) was pipetted into the wells of a white 96-well microplate, and 5 µL of each thawed sample was added into two wells containing the buffer. Then 100 µL of ATP Assay Mix (Sigma-Aldrich, St. Louis, MO, USA), diluted 100× with ATP Assay Mix Dilution Buffer (Sigma-Aldrich, St. Louis, MO, USA), was added to the diluted samples in the microplate wells. Luminescence emission (RLU_{sample}) was measured immediately using a Cytation 3 microplate reader (Biotek Instruments, Winooski, VT, USA). Ten µL of ATP (2×10^{-6} mol L^{-1}) was then added as an internal standard and luminescence was recorded again ($RLU_{ATP\ standard}$). The concentration of ATP in each sample (C_{ATP}, in µg mL^{-1}) was calculated according to the following equation:

$$C_{ATP} = \frac{RLU_{sample}}{RLU_{ATP\ standard}} \times C_{ATP\ standard}$$

where $C_{ATP\ standard}$ is the concentration of ATP standard in the reaction mixture, in µg mL^{-1}. Three biological replicates were each measured in four technical replicates.

2.6. ENM uptake and depuration experiments

T. thermophila cells exposed to ENMs as described above were sampled for cell counts and microscopic imaging at 30, 45 and 60 minutes. At each time point, the content of each well was mixed by gentle pipetting twice immediately prior to transferring 200 µL into a sterile 1.5 mL tube. The contents of the tubes were fixed with glutaraldehyde (2.5 % by volume), kept at room temperature for 30 minutes and then stored at 4 °C until cell counting and microscopic imaging.

After 60 minutes of exposure to ENMs, the protozoa were separated from the uninternalized nanomaterials and fecal pellets by centrifugation in iodixanol (OptiPrep™) density gradient medium as described previously.[34] Briefly, the protozoan samples were pipetted from the wells of the 12-well plate into 15-mL polypropylene centrifuge tubes and centrifuged for 5 minutes at 676×g, 4 °C using a swinging bucket rotor. Most of the supernatant was then pipetted away, leaving behind approximately 0.5 mL for pellet resuspension. The resuspended cells were then gently pipetted onto 2 mL of 10 % iodixanol in a 15-mL polypropylene centrifuge tube and centrifuged for 5 minutes at 1864×g, 4 °C. The protozoa and fecal pellets concentrated at the bottom of the tube, while the ENMs were in the upper layers of iodixanol as determined previously.[34] Most of the iodixanol layer was pipetted away carefully to avoid remixing, then 0.5 mL of Dryl's medium was pipetted into the tube for pellet resuspension. The resuspended samples were then gently pipetted onto 2 mL of 20 % iodixanol in 15-mL polypropylene centrifuge tubes and centrifuged for 5 minutes at 1864×g, 4 °C. The protozoa formed a layer on top of the 20 % iodixanol and the fecal pellets were at the bottom of the tube. Therefore, 2 mL of the top layer, containing protozoa, were pipetted into a clean 15-mL tube, mixed with 10 mL of Dryl's medium by gently inverting the tube and then centrifuged for 5 minutes at 676×g at 4 °C. The supernatant was removed, and the pellets were resuspended in 1 mL of Dryl's medium and transferred to the wells of a 12-well plate. The tubes were rinsed with 1 mL of Dryl's medium and added to the wells, bringing the final volume in each well to 2 mL. The protozoa in the depuration medium were sampled, by pipetting 100 µL from each well, immediately after the density gradient centrifugation and after 30, 45, 60, 120 and 180 minutes of incubation in a humidity chamber at 30 °C. The samples were fixed with glutaraldehyde (2.5 % by volume), kept at room temperature for 30 minutes, and then stored at 4 °C until cell counting and microscopic imaging.

2.7. Microscopy and imaging of ENMs in *T. thermophila*

For the preparation of the microscopy slides, the fixed protozoan samples, stored at 4 °C, were centrifuged for 10 minutes at 1000×g. The supernatant (120 µL) was removed, leaving ~50 µL for pellet resuspension. Five µL of the concentrated *T. thermophila* suspension was pipetted onto an ethanol-cleaned glass microscopy slide, followed by 5 µL of Mowiol 4-88 (Sigma-Aldrich, St. Louis, MO, USA) solution, mixed by pipetting and covered with an ethanol-cleaned glass coverslip. The slides were left to harden at room temperature for 24 h, then stored at 4 °C until imaging. The cells were imaged using an Olympus BX51 upright microscope, with differential interference contrast (DIC) optics (Nomarski microscopy), using a 100× oil immersion objective. The images were captured using a Retiga 2000R QImaging Camera and the Q-Capture Pro 7 software (Surrey, BC, Canada). Each cell was imaged at several focal planes to capture all ENM-filled food vacuoles in the cell. Twenty to thirty (20 to 30) cells were imaged per sample.

2.8. Image analysis

Initially, the images captured from the same cell at different focal planes were overlayed in Photoshop and the opacity of the layers was adjusted so that all filled food vacuoles were in focus and visible in one image. The resulting images were analyzed in ImageJ to determine the areas of filled food vacuoles per cell. Under the "Analysis" tab, the scale was set to indicate the number of pixels corresponding to one micrometer in the image and the image type was set as 8-bit. Then the area of the protozoan cell was determined using a freehand drawing tool and the "Analyze → Measure" function. To quantify the areas of food vacuoles in the cell, the images were converted to binary images by adjusting the threshold so that filled food vacuoles appeared black in the white background. Food vacuoles of one cell were surrounded using a freehand selection tool to exclude any black areas in the binary image (other than food vacuoles) from the analysis. The area of the food vacuoles was determined using the "Analyze Particles" tool. Where BN-filled vacuoles did not have sufficient contrast to outline filled food vacuoles accurately in the binary images, food vacuoles were manually outlined using a brush tool prior to quantifying the food vacuole area.

2.9. Conversion of food vacuole areas to masses of ENMs per dry weight of protozoa

The areas of ENM-filled food vacuoles obtained by image analysis were converted to mass of ENM per dry weight of protozoa. The following assumptions were made: (i) the total ENM area in the cell was equal to the sum of filled food vacuole areas in the cell; thus, the area of an "average" food vacuole was calculated by dividing the total area of ENM-filled food vacuoles by the number of filled food vacuoles per cell; (ii) food vacuoles had a spherical shape; the projected area of the average food vacuole was assumed to be circular, and was converted to the volume of an average food vacuole using the equation for the volume of a sphere; and (iii) the dry weight of the protozoan cell was approximately 1860 pg, as per Mielke et al., 2013.[29] The ENM mass concentrations in protozoa were calculated as described previously,[29] with the modification of using tapped densities of ENMs instead of true material densities. The tapped densities of the ENMs were measured according to the method of the International Pharmacopoeia which defines tapped density of a powder as an increased bulk density attained after mechanically tapping a container holding the powder sample.[35] The tapped density of ENMs was assumed to be representative of the density of ENMs "packed" in the protozoan food vacuoles upon ingestion because it would take into account not only the density of the ENMs but the void volume between the ENMs which was expected to be different for tubular, planar and spherical ENMs employed in this study. The tapped densities of ENMs were measured by filling a 25-mL pre-weighed glass cylinder with ENM powder up to 1-mL line while tapping until the volume of the ENMs in the cylinder remained constant, then weighing again to determine the mass of the ENMs. To calculate the ENM mass per cell, the tapped density was multiplied by the volume of the "average" food vacuole and the number of food vacuoles in the cell. Finally, the ENM mass per dry weight of protozoa was obtained by dividing the ENM mass per cell by the sum of the dry weight of the cell plus ENM mass per cell.

2.10. Calculation of uptake and depuration rate coefficients

The uptake and depuration rate coefficients (k_1 and k_2, respectively) were calculated using the sequential method reported in the OECD guideline 305, Annex 5.[36] The first order rate coefficients of depuration (k_2 in h^{-1}) were derived from the slopes of the linear regression of ln(ENM concentration in protozoa) *versus* time. The rate coefficients of uptake, k_1 in L kg^{-1} dry weight (dw) h^{-1}, were estimated based on nonlinear model fitting in Excel, using derived k_2 values and the equation:

$$C_p = \frac{C_w k_1}{k_2}\left(\mathbf{1} - \boldsymbol{e}^{-\boldsymbol{k_2 t}}\right),$$

where C_p (mg kg^{-1} dw) is the ENM concentration in protozoa at time t (h) and C_w (mg L^{-1}) is the ENM concentration in water (Dryl's medium).

2.11. Fractal dimension analyses of CB-, GNP- and CNT-filled food vacuoles

Fractal dimension analyses were applied to characterize the shapes of the food vacuoles of the *T. thermophila* cells exposed to ENMs for 60 minutes. The images of protozoa with CB-, GNP- and CNT-filled food vacuoles were converted into binary images as above, and the ImageJ plugin Fraclac[37] was used to describe the morphology of the filled food vacuoles.[38] A box-counting method was used, in which the fractal dimension (D_f) of the irregular shapes is determined by the slope of the least square linear fit of the log-log plot of *n* and box size, where *n* is the "number of non-overlapping equal boxes needed to cover the outline of the shape".[39] In the built-in FracLac plugin of Image J, there was a total of 12 box sizes increasing linearly with a minimum size of 1 pixel and a maximum size of 45 % of the image size. The intermediate box sizes were autoselected by the FracLac program. A minimum grid size of 1 pixel allowed for a detailed analysis of the morphology of the vacuoles. Ten cells per each ENM treatment were analyzed.

2.12. Statistical analysis

Uptake and depuration experiments were conducted in three independent replicates, i.e., on three different days with freshly cultured and prepared protozoa. In each independent replicate experiment, 20 to 30 protozoan cells per ENM treatment and per time point were analyzed by microscopy and image analysis. Statistically significant differences of the means were determined using either one-way analysis of variance (ANOVA) or a two-tailed Student's t-test (Microsoft Excel, Microsoft Corporation, Redmond, WA, USA). The values reported are the means of 3 replicates ± standard deviation derived by error propagation.[40]

3. Results and discussion

3.1. ENM dispersion and characterization, and test design considerations

Unfunctionalized hydrophobic carbon- and BN ENMs were dispersed using a previously optimized protocol employing probe sonication in alginic acid solution.[31] Alginic acid, a natural polysaccharide found in the cell walls of brown algae and secreted by certain environmental bacteria, was used herein as a suitable dispersant for ENMs, enabling the preparation of well-dispersed ENM stocks in Nanopure water and subsequent ENM dilutions in Dryl's medium. It was also confirmed

Table 1. Nanomaterial physicochemical characteristics.

Nano-material	Catalog #	Size, nm[a]	Size, nm[b]	Aspect ratio[c]	SSA, $m^2 g^{-1a}$	Purity, wt.%[a]	HDD, nm (Z-potential, mV) in Nanopure water[d]	HDD, nm (Z-potential, mV) in Dryl's medium[d]
CNT	Sku-030106	Diameter: 30–50, length: 10000–20000	Diameter: 21 ± 7	714	60	>95	171 ± 2 (-53 ± 1)	176 ± 2 (-35 ± 1)
GNP	GNP Grade 3	Diameter: 2000, thickness: 8–12	Diameter: 1225 ± 797, thickness: 5 ± 3	245	600–750	>97	212 ± 7 (-49 ± 2)	178 ± 4 (-29 ± 0.3)
hBN	255475 *Aldrich*	Diameter: 1000	Diameter: 306 ± 504, thickness: 7 ± 5	44	N/A	98	351 ± 53 (-65 ± 1)	330 ± 33 (-40 ± 0.4)
BNNT	802824 Aldrich	Diameter: 5 ± 2, length: 10000	Diameter: 15 ± 9	667	>100	>50	189 ± 6 (-57 ± 1)	457 ± 42 (-35 ± 1)
CB	PRINTEX® 30	N/A	Diameter: 37 ± 8	1	72	>99	177 ± 2 (-55 ± 0.5)	137 ± 8 (-39 ± 3)

[a]reported by the manufacturer; [b]after dispersion with alginic acid, measured using transmission electron microscopy (TEM) or atomic force microscopy (AFM) as reported previously;[31, 41] [c]calculated by dividing mean length by measured diameter (for CNT and BNNT) and by dividing the measured lateral size by thickness (for GNP and hBN); [d]measured using a Zetasizer Nano ZS-90 (Malvern Instruments Ltd.) immediately after dispersing ENMs in aqueous media at 10 mg L^{-1} as reported previously;[31] SSA – specific surface area; HDD – hydrodynamic diameter; CNT – multiwall carbon nanotubes; GNP – graphene nanoplatelets; hBN – hexagonal boron nitride flakes; BNNT – boron nitride nanotubes; CB – carbon black; N/A – not available.

that alginic acid, at the concentration used in this study (20 mg L^{-1}), was neither toxic nor growth-stimulatory to *T. thermophila*.[31] The physicochemical characteristics of ENMs have been reported previously.[31] Briefly, among the two planar ENMs employed in this study, GNPs had larger dimensions than hBN (Table 1), but both had thicknesses in the range of a few nanometers after exfoliation by sonication (data not shown). The two tubular ENMs, CNTs and BNNTs, had comparable diameters (~21 and 15 nm, respectively, Table 1) and lengths in the micrometer scale, as observed in TEM images.[31] Spherical CB particles had an average diameter of < 40 nm, as measured by TEM (Table 1). Thus, all ENMs were in the size range suitable for ingestion by *T. thermophila* which has an average cell size of 20 × 50 µm, and for potential accumulation in the protozoan food vacuoles which can be as large as ~3 µm in diameter as measured in the current study. Although some CNTs and BNNTs may have been longer than 3 µm, they were bent in shape and, once dispersed in the aqueous media, were confirmed to form agglomerates in the size range of ≤ 200 nm in Nanopure water and < 500 nm in Dryl's medium, based on dynamic light scattering (DLS) measurements (Table 1). GNPs, hBN and CB were also well dispersed in both Nanopure water and Dryl's medium, with average hydrodynamic diameters of 137-330 nm. The hydrodynamic diameters of CNTs, GNPs and hBN in Dryl's medium remained unchanged over 24 h, however, BNNTs formed ~7-µm agglomerates (Fig. S1). Although the uptake phase in the current study was shorter than 24 h (1 h), the data indicated that BNNTs had a higher tendency to agglomerate in Dryl's medium than other ENMs. However, phagocytosis was confirmed for all ENMs.

The concentration of ENMs for the uptake experiments was chosen to meet the following conditions: (i) non-toxic to *T. thermophila*, (ii) would not be too high to obstruct imaging of intracellular food vacuoles, i.e., ENMs would not form large agglomerates and coat the cell surface, and (iii) would not be too low to become a limiting factor of ENM uptake during the uptake phase. It was confirmed experimentally that 10 mg L^{-1} would satisfy these requirements in the case of all ENMs. Specifically, incubation of *T. thermophila* in Dryl's medium, which is a mineral medium that does not support growth, amended with 10 mg L^{-1} of ENMs did not affect the protozoan cell concentration or viability over 1 h, i.e., the duration of the uptake phase (Fig. 1).

3.2. Inter-individual variability in ENM uptake and depuration in the protozoan populations

Food vacuoles filled with ENMs were apparent from Nomarski (DIC) micrographs of protozoa exposed to the various ENMs, but food vacuoles were not visible in the images of untreated protozoa (control) due to exposures in starvation media (Fig. 2A). The three carbon-based ENMs were readily detectable in the filled protozoan food vacuoles, occurring in images as dark agglomerates (Fig. 2B-D). In stock dispersions, hBN and BNNT appeared white and brown, respectively (not shown). However, Nomarski microscopy allowed detection of hBN and BNNT-filled food vacuoles due to their opacity and higher contrast compared to the rest of the cell (Fig. 2E, F). Internalized ENMs that appeared as densely packed ENM agglomerates inside the food vacuoles were clearly distinguishable from extracellular ENM agglomerates that were less dense and thus had lower contrast in micrographs (Fig. 2, black arrows).

The micrographs indicated an increase in the number of ENM-filled food vacuoles in *T. thermophila* during 1 h of uptake (Fig. 2B-F). The average number of ENM-filled food vacuoles per protozoan cell increased linearly between 30–60 minutes of uptake, indicating that ENM concentration was not a limiting factor of the active phagocytosis of ENMs by *T. thermophila*. The average number of ENM-containing food vacuoles per cell increased from 2 ± 2 (range

0–15) at 30 minutes to 5 ± 3 (range 0–15) at 45 minutes and 8 ± 3 (range 0–22) at 60 minutes, although these averages did not differ significantly across the different ENM treatments.

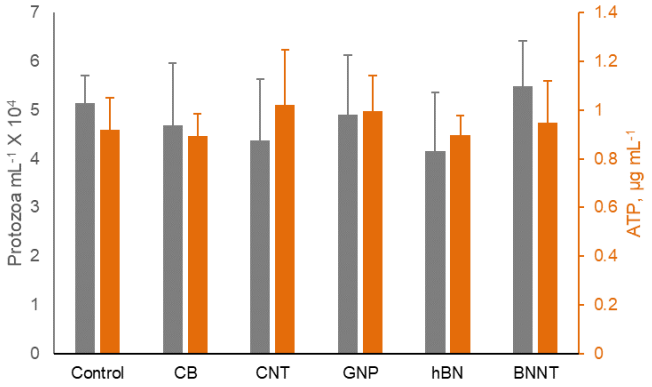

Fig. 1. Total protozoan cell concentration and ATP content of the culture after 1-h incubation with and without ENMs (10 mg L^{-1}) in Dryl's medium (non-growing culture). ENMs did not induce significantly different (one-way ANOVA, $F < F_{crit}$, i.e., the means of datasets are equal) changes in the cell count ($P = 0.423$) or ATP content ($P = 0.283$) compared to unamended control. Values are mean ± standard deviation (n = 3). CB – carbon black, CNT – multiwall carbon nanotubes, GNP – graphene nanoplatelets, hBN – hexagonal boron nitride flakes, and BNNT – boron nitride nanotubes.

However, the total number of food vacuoles in individual cells at each time point varied considerably, leading to the formation of sub-populations with different numbers of ENM-filled food vacuoles (Fig. 3A-C). While, expectedly, the percentage of cells with higher vacuole numbers increased and the percentage of empty cells decreased during the uptake phase, it was interesting that even after 60 minutes of exposure to ENMs there was a certain fraction of cells which did not contain any food vacuoles (Fig. 3C). Intercellular variability in the uptake of ENMs by *T. thermophila* was recently demonstrated in a population exposed to low concentrations (ng L^{-1}) of Au NPs.[22] In the exposure conditions where the NP concentration was the limiting factor for uptake, it was demonstrated that Au NPs were internalized only by a small number of cells while the majority of the protozoan population remained devoid of NPs after 24-h exposure. Such accumulation of ENMs in the small fraction of the protozoan population suggested that the fittest members of the population might have ingested the available NPs, exhausting the NP supply or reducing the frequency at which the remaining population encountered and ingested NPs. However, the experiments herein indicated that the variability in ENM uptake among individual protozoan cells was not solely attributable to the availability of ENMs or the likelihood of the cells encountering ENMs in the medium, since here ENMs were provided at a sufficiently high concentration (10 mg L^{-1}). Rather, such intercellular variability in food vacuole formation must have been caused by the physiological differences between the protozoa. Similar inter-individual variability in microplastic particle ingestion rates was recently reported in juvenile anemonefish and demonstrated to be correlated with the individual activity levels of fish.[42] It was concluded by the authors that phenotype-dependent microplastic ingestion could have population- and community-level consequences due to more active individuals being at higher risk of pollutant exposure which may interrupt predator-prey interactions. Whether the variability in ENM uptake among individual protozoan cells also correlates with their phenotype remains to be investigated.

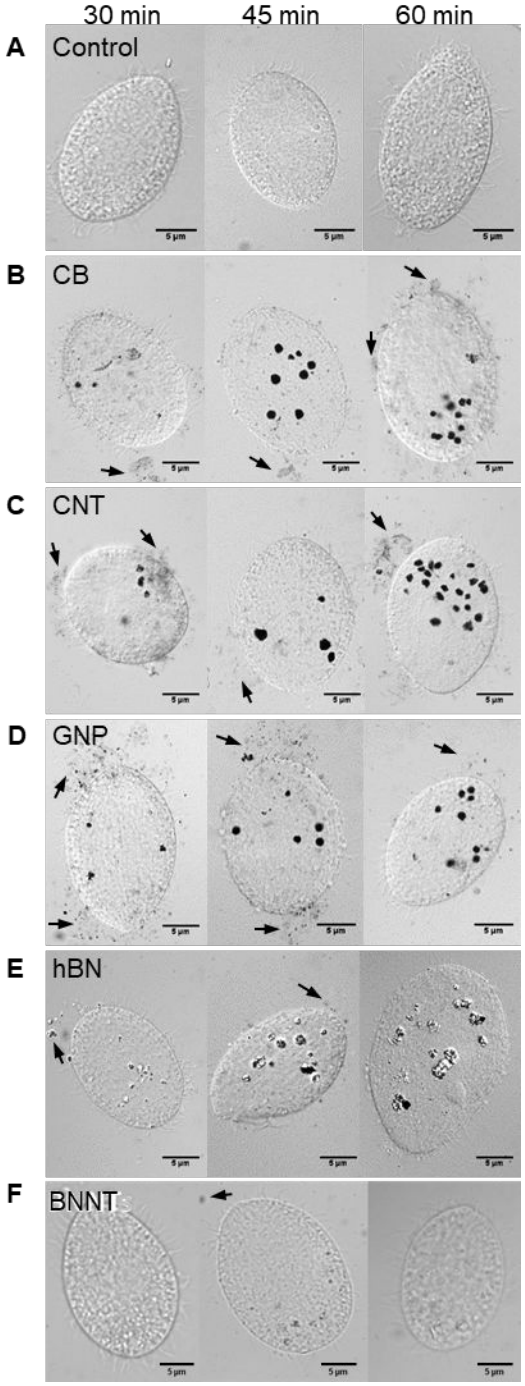

Fig. 2. Nomarski, or differential interference contrast (DIC), microscopy images of *T. thermophila* after incubation (A) without or (B-F) with ENMs (10 mg L^{-1}) for 30, 45 or 60 minutes in Dryl's medium. ENM agglomerates internalized by phagocytosis appear as (B-D) dark or (E-F) optically dense areas in the food vacuoles. Extracellular ENM agglomerates (black arrows) are less dense and have lower contrast than phagocytosed ENMs. Scale bars: 5 µm. CB – carbon black, CNT – multiwall carbon nanotubes, GNP – graphene nanoplatelets, hBN – hexagonal boron nitride flakes, and BNNT – boron nitride nanotubes.

ARTICLE

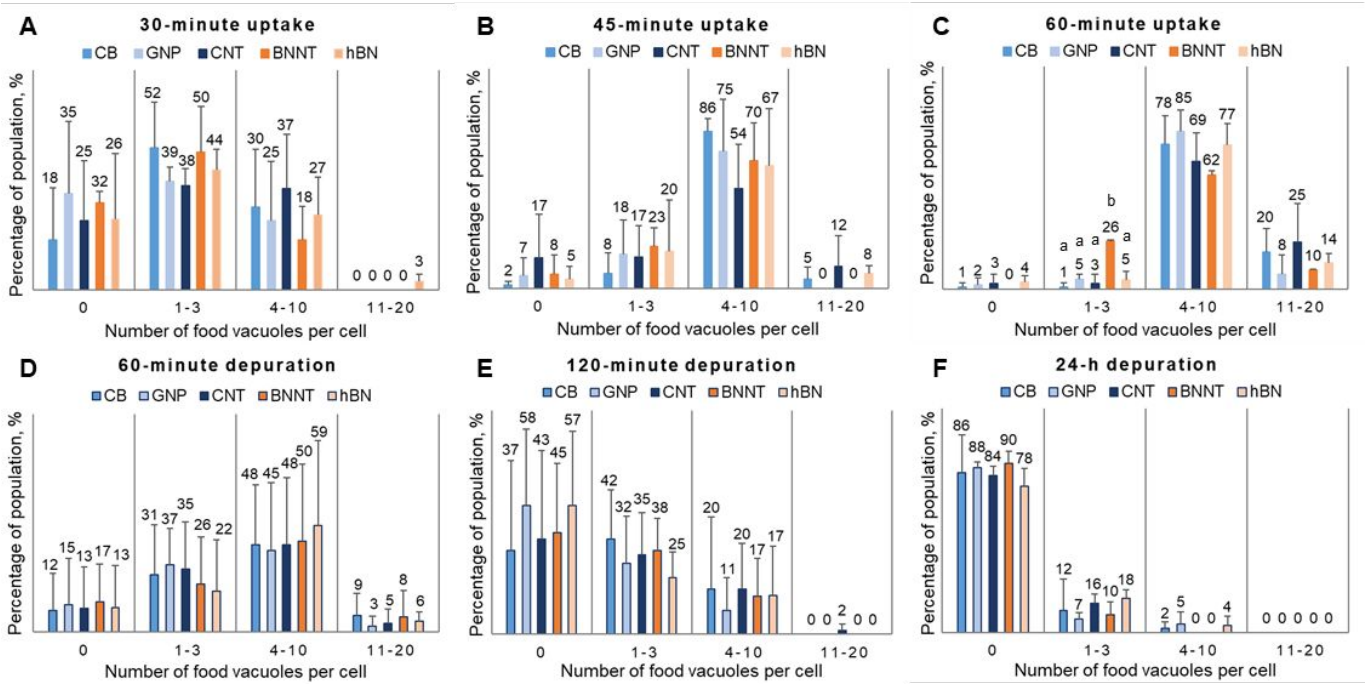

Fig. 3. The percentages of the protozoan population in arbitrarily assigned categories of total food vacuole numbers per cell (i.e., 0, 1-3, 4-10 or 11-20) upon exposure to ENMs for (A) 30, (B) 45 and (C) 60 minutes and after depuration for (D) 60 and (E) 120 minutes and (F) 24 h. Data labels indicate percentages of population and similar letters indicate no statistically significant differences ($p > 0.05$, ANOVA and t-test) within the x-axis category. No letters mean that there are no statistically significant differences ($p > 0.05$, ANOVA) between the data within the x-axis category. Data are the mean of three independent experiments ± SD.

It was expected that there would be no differences in the food vacuole numbers formed in the different ENM treatments because it has been established before that *T. thermophila* indiscriminately grazes on different types and sizes of ENMs, from quantum dots with the primary size of 5–12 nm[32, 43] to metal oxide NPs that can agglomerate in aqueous media, forming particles with hydrodynamic diameters of ~200 nm – ~1200 µm,[29, 44] and to CNTs that formed agglomerates in the size range of ~200 nm – ~1500 µm.[18] Further, comparison of uptake of 10 nm and 20 nm Ag NPs or Au NPs by *T. thermophila*, quantified by hyperspectral imaging microscopy, confirmed that uptake of NPs did not depend on the primary particle size.[27] This is in accordance with the behavior of phagotrophic protists in natural environments, where they graze on bacteria and other particulate matter to obtain nutrients with no lower limit in ingested particle size. Thus, as long as the particles remain below the upper size limit which has been estimated to be somewhere in the range of 2.4–10 µm,[45] the uptake should not be affected by ENM type or size.

Similarly to the uptake phase, there was also variation in food vacuole numbers per cell in the depurating protozoan populations (Fig. 3D-F), again with no significant difference between ENM treatments. While after 60 minutes of depuration the highest percentage of protozoan cells still contained 4 to 10 filled food vacuoles and only between 12–17 % of cells were completely devoid of ENMs (Fig. 3D), by 120 minutes of depuration the distribution was roughly reversed, with the majority of the cells being ENM-free (37–58 % of the population) and ~11–20 % of protozoa containing 4 to 10 filled vacuoles (Fig. 3E). However, after 24 h, while the majority of the cells were cleared of ENMs, remarkably, 7–18 % of the population still contained 1 to 3 filled food vacuoles, while in the case of protozoa exposed to CB, GNPs or hBN, 2–5 % of cells included as many as 4 to 10 ENM-filled vacuoles (Fig. 3F). Similarly long-term trends in intracellular persistence of ENMs in *T. thermophila* were reported in the case of QDs;[43] however, due to the small size of the QDs (12 nm), it was concluded that the non-depurated particles may have entered protozoan cells via alternative pathways to phagocytosis, and thus were not depurated. In the current study, ENMs were not small enough to enter the cells by endocytosis or pinocytosis, thus must have been retained in phagosomes or lyso-phagosomes.

3.3. ENM mass per individual cells was ENM-dependent.

The assumption that internalized ENMs, once taken up and prior to depuration, were confined to the food vacuoles was based on a prior study where a significant linear correlation was established between the CNT mass (quantified using ^{14}C-labeled CNTs) per cell *versus* CNT area per cell as measured in the Nomarski microscopy images[18] (Fig. S2A). Thus, it had been previously established that the amounts of CNTs in apparently filled food vacuoles were estimable from micrographs.[18] Here, there wasn't an effect of ENM type on the total numbers of food vacuoles at any given time (Fig. 3), but the sizes of food vacuoles appeared to vary (Fig. 2). This meant that the simple count of filled food vacuoles would not accurately reflect the mass of ENM phagocytosed. Rather, the sizes and numbers of filled food vacuoles had to be taken into account. Here, ENM areas per cell as quantified in micrographs were converted to mass-based ENM concentrations as described in the Materials and Methods, including adjusting the calculations for the densities of the various ENM types studied herein. For this, total areas of ENM-filled food vacuoles per cell (μm^2) were used in the calculations of ENM mass per cell (mg) and the "packing" density of ENMs in the food vacuoles was simulated by determining the tapped densities of the ENMs as described in Materials and Methods. The tapped densities (Table 2) allowed taking into account not only the density of the ENM but the void volume between the ENMs in the vacuoles. The accuracy of the image analysis-based ENM mass calculation approach used herein was confirmed by comparing the calculated CNT masses per cell to the previously determined CNT masses per *T. thermophila* cell using analytical measurements of ^{14}C-labeled CNTs.[18] The calculations based on the CNT areas per cell in this study yielded CNT masses per cell (Fig. S2B and C) which were in the same order of magnitude as previously analytically measured CNT masses (Fig. S2A),[18] confirming the accuracy of the image analysis and calculation-based approach in the current study.

Table 2. Measured and literature-reported tapped densities and literature-reported material densities of ENMs.

Nano-material	Measured tapped densities ($g\ cm^{3\ -1}$)*	Tapped densities from literature ($g\ cm^{3\ -1}$)	Material densities ($g\ cm^{3\ -1}$)
CB	0.258	0.38;[46] 0.34[47]	1.8-2.1[48]
CNT	0.154	0.12;[49] 0.22[50]	2.1[51]
GNP	0.369	0.2-0.4[52]	2.3[53]
hBN	0.499	N/A	2.3 (BN)[54]
BNNT	0.033	N/A	2.3 (BN)[54]

*The coefficient of variation (CV) of tapped density measurements was < 3%; N/A – not available

Differently from the food vacuole numbers in protozoa (Fig. 3), the calculated ENM masses based on micrograph measurements and conversions that included tapping density indicated statistically different ENM contents in protozoa exposed to different types of ENMs (Fig. 4). Specifically, significantly higher percentages of cells contained lower masses of BNNTs, and higher masses of hBN, compared to other types of ENMs during the uptake phase (Fig. 4A-C). Similar trends were observed after 60 and 120 minutes of depuration; however, the differences were not significant in some cases due to large variations in the data (Fig. 4D-F). The apparent difference in the food vacuole number-based data (Fig. 3) and the ENM mass-based data (Fig. 4) indicated that even though the ENMs were ingested with similar rates based on the formation of food vacuoles, the resulting intracellular mass of the ENMs differed by ENM type due to their different "packing" densities in the vacuoles. The amount of ENMs in a food vacuole was thus determined by the shape of the ENM which influences its tapped or "packing" density. Since the shape of ENMs appeared to affect the mass of ENM per protozoan cell, we next sought to determine if the kinetics of ENM uptake and depuration were similarly affected by ENM shape.

3.4. ENM uptake and depuration kinetics

To quantitatively characterize the uptake and depuration of ENMs (Fig. 5), a biodynamic approach was used to derive uptake and depuration rate coefficients (k_1 and k_2, respectively, Table 3). A dynamic model was employed because, unlike in static models based on the measured chemical concentration in organisms and the exposure medium, the assumption of the equilibrium partitioning theory[11] does not have to be met, and thus is applicable for ENMs.[10] It is worth noting that instead of the commonly used terminology of "elimination", which is defined as "the combined process of metabolism, excretion, and degradation which results in ENM removal from an organism",[12] the term "depuration" is used here because no metabolism or degradation of the carbonaceous and BN-based ENMs is expected during the relatively short exposures employed here; also, the CNTs were previously shown to be confined within the food vacuoles (i.e., the "digestive tract" of protozoa) and not pass into the cytoplasm as established previously.[18] The simple one-compartment model was considered adequate because (i) only one type of uptake of ENMs, i.e., active phagocytosis, similarly to the filter-feeding process of higher organisms, was assumed due to the organism physiology and the hydrodynamic sizes of the ENMs; (ii) unlike in the case of metal ENMs, no chemical or biological transformations of ENMs were expected to occur which would affect the biodistribution or elimination kinetics of ENMs in the organism; and (iii) no change in the biomass of the organisms occurred during the uptake and depuration phases because the experiments were conducted in a medium which did not support protozoan growth—confirmed by no significant changes in the cell sizes and concentrations during the experiments (data not shown). Additionally, the calculated ENM concentrations in the exposure media at the end of the 1-h uptake phase were in the range of 7.6–9.9 mg L^{-1}, indicating that ENM concentration was not considerably reduced from the starting concentration of 10 mg L^{-1}. This confirmed that ENM concentration was not a limiting factor for ENM uptake in protozoa.

The ENM concentration in protozoa increased from 0 to 1 h, and steady state was not reached as evidenced from the uptake curves which did not reach a plateau by 1 h (Fig. 5A, C, E, G, I). At 1 h, protozoa had internalized 4400 ± 1700 mg kg^{-1} dw of CB, 4800 ± 2200 mg kg^{-1} dw of CNTs, and 3800 ± 1300 mg kg^{-1} dw of GNPs, which did not differ significantly across the ENMs ($p > 0.05$, ANOVA). However, the concentration of hBN in protozoa after 1-h uptake was significantly higher (10,200 ± 5200 mg kg^{-1} dw), and of BNNT significantly lower (560 ± 240 mg kg^{-1} dw), compared to the carbon-

ARTICLE

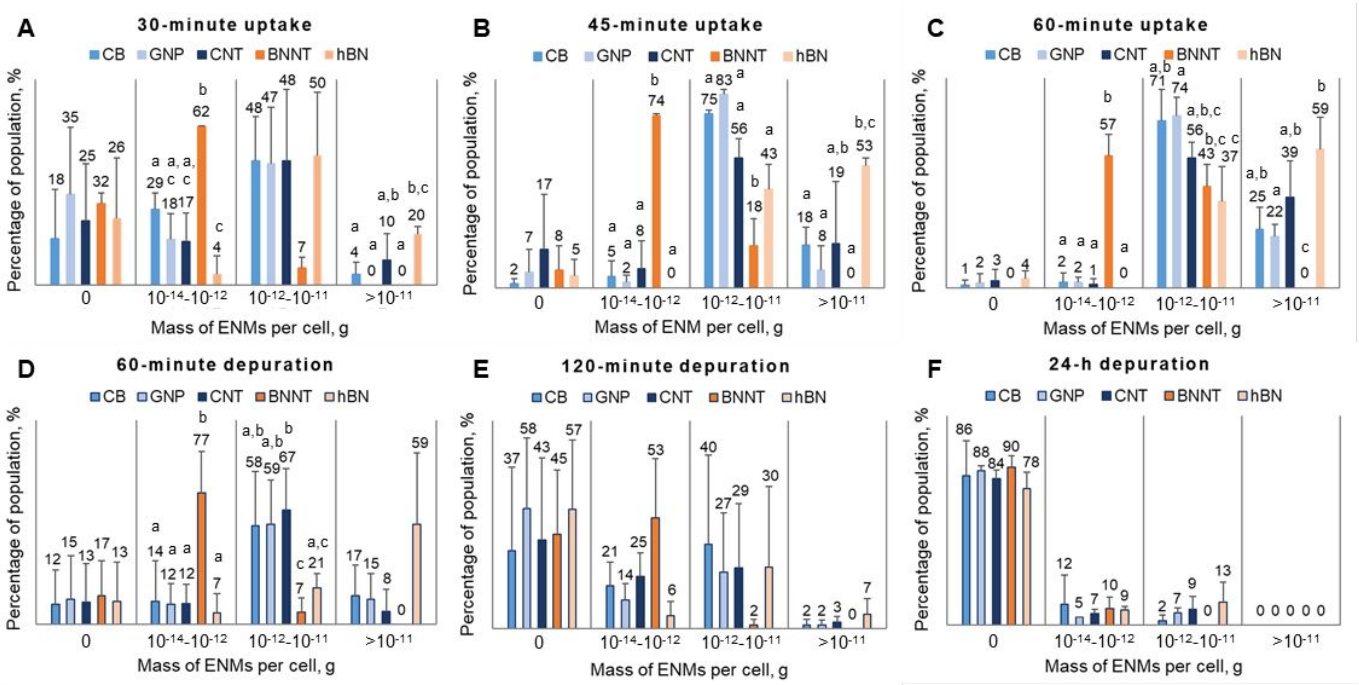

Fig. 4. The percentages of the protozoan population in arbitrarily assigned categories of ENM mass per cell (i.e., 0, 10^{-14}-10^{-12}, 10^{-12}-10^{-11} and >10^{-11} g) upon exposure to ENMs for (A) 30, (B) 45 and (C) 60 minutes and after depuration for (D) 60 and (E) 120 minutes and (F) 24 h. Data labels indicate percentages of population and similar letters indicate no statistically significant differences ($p > 0.05$, ANOVA and t-test) within the x-axis category. No letters mean that there are no statistically significant differences ($p > 0.05$, ANOVA) between the data within the x-axis category. Data are the mean of three independent experiments ± SD.

based ENMs. These differences are explainable by the different tapped densities of BN-based ENMs than those of the carbonaceous ENMs (Table 2). Even though the uptake phase here was only for 1 h, it was assumed that depuration had occurred during the uptake phase, because literature-reported food vacuole processing times of *T. thermophila* range from 30 minutes to 2 h,[55] thus the sequential calculation of k_1 and k_2 was justified. The uptake rate coefficients were determined to be similar for all three carbonaceous ENMs, but significantly higher for hBN and significantly lower for BNNTs compared to carbon-based ENMs (Table 3). There are only a few studies that have used kinetic models to characterize bioaccumulation of non-soluble ENMs in environmental model organisms. Thus, the ENM uptake rate coefficients for these organisms are presented here for comparison, even though they have a different physiology than protozoa which likely affects ENM ingestion. Uptake rate coefficients (k_1) of CNTs in zebrafish *Danio rerio* were reported to be ~10 L kg^{-1} h^{-1} [56] and in green microalgae 85 L kg^{-1} h^{-1},[57] both values modeled using a one-compartment kinetic model. The same modeling approach was also used to describe the uptake of TiO_2 NPs in waterborne exposure of nematodes, resulting in the kinetic uptake rate coefficients ranging between ~ 10–240 L kg^{-1} h^{-1}, depending on the biological replicate experiment.[58] Thus, the uptake rate coefficients determined in the current study for *T. thermophila* are in the similar range (considering the relatively large variability of the data) or slightly higher, in the case of hBN (Table 3).

Depuration rate coefficients (k_2) were calculated separately for 1 h and 2 h of depuration (Table 3). The one-hour k_2 was used for modeling the uptake rate coefficient (k_1), since the uptake phase lasted for 1 h. However, since the majority of the ENMs were depurated from the protozoa by the end of 2 h, two-hour k_2 values were calculated to characterize the depuration of ENMs. For comparison, CNTs which accumulated in the zebrafish gut had an elimination rate coefficient of 0.14 h^{-1},[56] and the growth-corrected elimination rate coefficient of CNTs in a growing culture of green microalgae was 0.008 h^{-1}.[57] The elimination rate coefficient of TiO_2 NPs in nematodes was ~0.4 h^{-1}.[58] These k_2 values are lower than the depuration rate coefficients determined in the current study, likely due to physiological differences of the organisms and also longer elimination phases used in the other studies (24–72 h) than here (2 h). Here, protozoa had depurated 76–93 % of the total ENM body

ARTICLE

Table 3. ENM uptake (k_1) and depuration (k_2) rate coefficients (mean ± STDEV; n = 3) calculated over 1 h of uptake and 1 or 2 h of depuration, respectively, percentages of ENMs in protozoa after 2-h and 24-h depuration, the body burden of ENMs in protozoa after 24-h depuration (mean ± propagated error, n = 2) and bioconcentration factors (BCFs).

Nano-material	k_1, L kg^{-1} dw h^{-1} (1 h)	k_2, h^{-1} (1 h)	k_2, h^{-1} (2 h)	% ENM retained in protozoa* after depuration for		Body burden after 24 h depuration, mg kg^{-1} dw	BCF, L kg^{-1}, (k_1/k_2)
				2 h	24 h		
CB	292 ± 6[a]	0.90 ± 0.6	1.45 ± 0.9	12 ± 12	0.6 ± 0.9	65 ± 268[a, b]	323
CNT	399 ± 186[a, b]	0.53 ± 0.4	1.08 ± 0.5	16 ± 9.2†	9 ± 12	100 ± 195[a, b]	755
GNP	276 ± 117[a]	0.96 ± 1.4	1.53 ± 0.9	11 ± 10	1.4± 0.7†	69 ± 171[b]	287
hBN	856 ± 239[b]	0.72 ± 0.1	1.57 ± 0.7	7.4 ± 5.3	1.8 ± 0.3†	210 ± 407[a, b]	1184
BNNT	39 ± 9[c]	0.38 ± 04	0.92 ± 0.5	24 ± 19	1.3 ± 0.8	2.4 ± 6.2[a]	103

* % ENM retained in protozoa compared to the body burden after 1-h uptake and in the beginning of depuration, † significantly different values from zero ($p < 0.05$, one-sample t-test). Different letters indicate significantly different values in the column. No letters indicate no significant differences between the values in a column ($p < 0.05$; two-sample t-test).

burden taken up during the 1-h uptake phase by the end of 2-h depuration (Table 3). By 24 h of depuration, the remaining ENM body burden had reduced to ~0.6–9%, indicating further depuration of ENMs after 2 h but at a much slower rate. However, statistical analysis indicated that, due to large variability of the data, only the mean % CNT retained after 2h and mean % GNP and % hBN retained after 24h significantly differed from zero. Still, there existed a population of protozoa that did not fully depurate ENMs from the food vacuoles even after 24 h. Incomplete depuration of CNTs and graphene has been previously reported in the case of a filter-feeding crustacean *Daphnia magna*. It was shown that 60 % of graphene which had accumulated in *D. magna* during 24-h exposure at 100 µg L^{-1}, was retained in the organisms during the 10-h depuration phase.[59] Similarly, in another study, 46–100 % of graphene—depending on the exposure concentration (50–250 µg L^{-1})—remained in *D. magna* by the end of the depuration phase, while algae as a food source induced 100 % depuration.[60] Also, it was demonstrated that *D. magna* exposed to CNTs at 0.4 mg L^{-1} for 48 h were unable to excrete CNTs during the 24-h depuration period, while the addition of algae during depuration induced the release of 50–85 % of CNTs from the crustaceans.[61] In zebrafish, size-dependent retention of graphene has been reported.[62] While both smaller (~30 nm) and larger (~500 nm) graphene layers were taken up by the zebrafish, the larger ENMs were almost completely eliminated from the organisms in 12 h, and up to 70 % of the smaller particles was retained in fish by the end of the 120-h depuration phase. These studies suggest that retention of ENMs in the organisms' guts for prolonged time periods may occur, and depuration is highly dependent on food availability which is usually not abundant in natural environments.

3.5. Bioconcentration of ENMs

Bioconcentration factors (BCFs, calculated as a ratio of k_1 and k_2 at 1 h) indicated that most of the studied ENMs (CB, CNTs, GNPs and BNNTs) could not be considered bioaccumulative in *T. thermophila* according to the regulatory guidelines used by the U.S. Environmental Protection Agency[63] which define "bioaccumulative" compounds as the ones having BCF > 1000 L kg^{-1} (Table 3). The only ENM which had a BCF exceeding the threshold of 1000 L kg^{-1} was hBN, indicating that this material was taken up by the protozoa more efficiently than it was depurated. This was also reflected by the highest residual body burden in *T. thermophila* after 24 h of depuration compared to other ENMs. Although not exceeding 1000 L kg^{-1}, the BCF of CNTs was the highest among the carbonaceous ENMs and higher than the BCF of BNNTs. CNTs were also retained in the protozoa at the second-highest mass concentration after hBN, indicating a higher bioaccumulative potential for these two ENMs. In other studies where BCF has been calculated using the same approach as here (i.e., from the ratio k_1/k_2), CNTs were determined to have a BCF of 70 L kg^{-1} in zebrafish[56] and as high as 4722 L kg^{-1} in green microalgae,[57] illustrating the effect of physiology and modes of uptake and depuration of CNTs in these organisms. Namely, since CNTs mainly were accumulating in the zebrafish gut, they were efficiently depurated; however, in green algae, CNTs were internalized in the cytoplasm, resulting in slower elimination. High BCF values (> 5000 L kg^{-1}, a threshold for "very bioaccumulative" substances)[63] for CNTs have previously been reported for *D.*

magna[61, 64] and *T. thermophila*,[18] and for graphene in *D. magna* and *T. thermophila*;[19] however, these values were calculated as ratios of ENM concentrations in the organisms and the medium at the end or during the uptake phase of ENMs, and thus are not directly comparable to the BCF values obtained herein using the kinetic approach.

3.6. High aspect ratio ENMs had longer residence times in protozoa

Due to the large variability in the data from the biological replicate experiments, there were no statistically significant differences between different ENMs regarding the depuration rate coefficients and % ENM retained in the protozoa (Table 3). Still, certain trends emerged: the two tubular ENMs (CNTs and BNNTs), i.e, high-aspect ratio ENMs (Table 1), were depurated relatively more slowly than the lower aspect ratio ENMs: planar (GNPs and hBN) or spherical ENMs (CB) based on the 1-h and 2-h depuration rate coefficients (k_2, Table 3). Indeed, linear regression analysis showed significant correlation (P=0.03) between the first order 2-h depuration rate coefficients and ENM aspect ratios (Fig. S3). Also, after 2 h of depuration, CNTs and BNNTs were retained in protozoa at relatively higher levels than other ENMs (Table 3). By 24 h, CNTs were still retained at the highest level (~9 %), while BNNTs appeared to have been depurated to levels comparable to those for hBN and GNPs (~1.3 %). CB, declared non-bioaccumulative in aquatic environments due to its insolubility in water,[30] was retained in protozoa at the lowest levels (~0.6 %) after 24 h depuration. However, when the body burdens of ENMs at 24 h of depuration were compared based on the ENM mass concentrations in protozoa, hBN was present intracellularly at the highest and BNNT at the lowest levels, even though they were significantly different only from the body burden levels of GNPs (Table 3). The apparent, albeit not statistically significant, difference between the mass concentrations of the two BN materials retained in the protozoa was likely due to the different tapped densities of hBN and BNNTs (Table 2) which allowed more efficient packing of hBN in the food vacuoles. This resulted in greater intracellular masses of the hBN than BNNTs, highlighting the significance of the ENM shape in cellular uptake and accumulation.

Still, the relatively lower initial depuration rate coefficients (at 1 and 2 h; Table 3) indicated that the high-aspect-ratio ENMs (CNTs and BNNTs) had longer residence times in the protozoa as compared to the other ENMs (Fig. S3). To explore further if shape might have played a role in the slower depuration of ENMs, possibly due to changing the shape of the food vacuoles which might have affected their intracellular transport and consequently excretion of the content, fractal dimension analyses of the ENM-filled food vacuoles were carried out. The numerical values of fractal dimensions (D_f) measure shape complexity where the values close to 1 are characteristic of shapes with lower complexity, i.e., spheres in the case of food vacuoles; the corollary is that values higher than 1 indicate more complex and irregular shapes. Our measurements indicated that, as hypothesized, CNT-filled food vacuoles had higher irregularity (D_f = 1.12 ± 0.06) than GNP- or CB-filled food vacuoles (D_f = 1.06 ± 0.09 and 1.07 ± 0.10, respectively), indicating that the uptake of high aspect-ratio ENMs caused the formation of deformed food vacuoles which may have been associated with a hindered depuration process. The hBN or BNNT-filled food vacuoles were excluded from the fractal dimension analysis because of the lower contrast of the food vacuole shapes in the images, and thus less accurate food vacuole shape visualization.

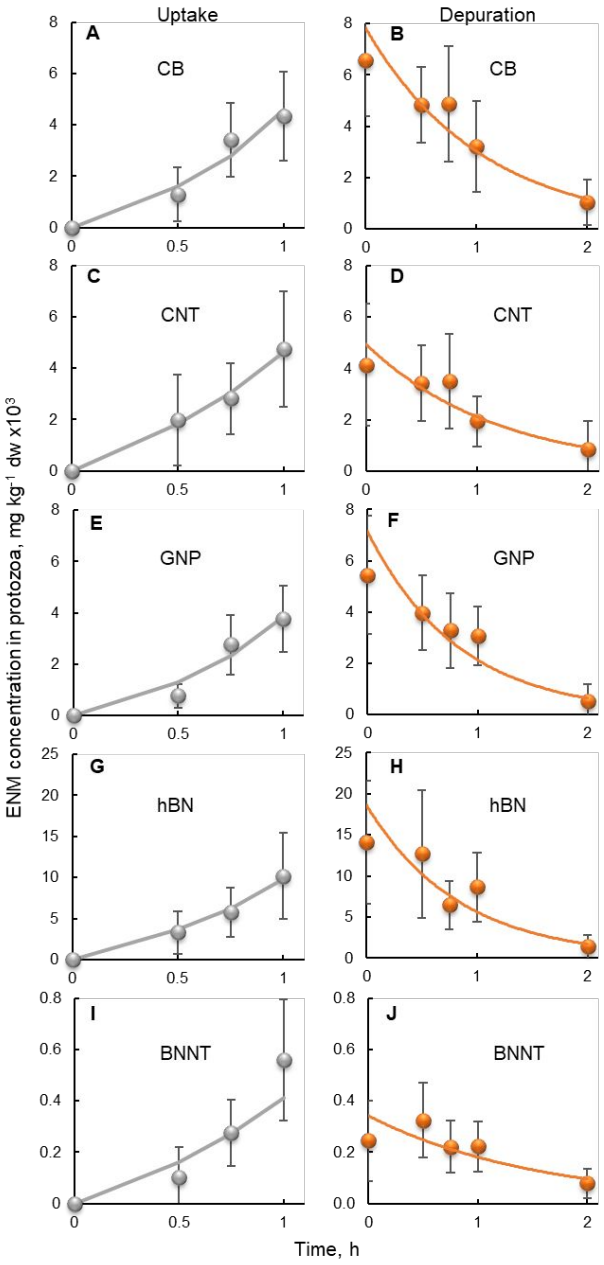

Fig. 5. Uptake and depuration kinetics of (A, B) carbon black, (C, D) multiwall carbon nanotubes, (E, F) graphene nanoplatelets, (G, H) hexagonal boron nitride flakes and (I, J) boron nitride nanotubes. The data points are mean ± propagated errors (n = 3). The lines in the uptake graphs indicate non-linear regression model fitting and the lines in depuration graphs are exponential trendlines.

The influence of ENM shape on ENM uptake and accumulation in invertebrate organisms has only been explored in a limited number of studies, and the results have varied from no effect of shape to preferential bioaccumulation of rod-shaped or tubular ENMs. For example, three separate studies conducted with the same set of CuO spheres, platelets and rods, but with a different sediment-dwelling

organism, demonstrated that, while deposit-feeding worms accumulated higher amounts of CuO rods than spheres or platelets,[7] there was no shape-dependence in the uptake and depuration of the CuO ENMs in freshwater gastropods[8] and sediment polychaeta.[9] Since CuO ENMs may dissolve to some extent, their bioaccumulation and distribution in the organisms may be affected by the dissolved copper and other chemical transformations of the ENMs. Thus, the results may not be comparable to the current study of carbon- and BN-based ENMs which are insoluble. Regarding shape-dependent bioaccumulation studies of insoluble ENMs, the distribution and accumulation of TiO_2 spheres and tubes were compared in paddy microcosms, and different bioaccumulation patterns were established for the two ENMs.[65] However, the reasons were unclear, and it was proposed that the bioaccumulation of differently shaped TiO_2 ENMs depended on the organism size, physiology and feeding pattern as well as the size and agglomeration extent of the ENMs.[65] Regarding carbon-based ENMs, their size-dependent uptake and elimination have been demonstrated in mammalian macrophages which, similarly to the ciliates used as model organisms here, internalize particulate matter by phagocytosis. The uptake of CNTs by macrophages was shown to increase linearly with the dynamic size of CNT bundles in the medium (ranging from ~ 30 to ~400 nm).[14] Another study demonstrated that the uptake of single-walled CNTs by macrophages did not depend on the length of the nanotubes as long as the CNTs were < 1 µm, but the exocytosis was shown to be length-dependent with longer CNTs being eliminated more slowly than shorter CNTs.[20] These studies indicate that the interactions of long fibrous ENMs with cells and subcellular compartments such as phagosomes relate to their physical properties, and are likely different from non-fibrous ENMs.

3.7. Broader implications

Similarly to ENMs studied here, microplastics are insoluble particulate materials, and their bioaccumulation studies are complicated by the lack of quantitative analytical methods and standard test designs. Also, the bioaccumulation of microplastic particles is driven by physical processes, not thermodynamic equilibria, and is dynamic, not steady state, due to particle agglomeration, dispersion, settling and other physico-chemical processes which affect particle interactions with the organisms.[10, 12, 66] Due to the difficulties with quantification, there is limited data on the uptake and depuration kinetics of microplastic particles. However, some published studies indicate that there may be a reason for concern, especially regarding the bioaccumulation of environmentally prevalent non-spherical secondary microplastics.[67-71] Novel single-cell-based methods for uptake and depuration quantification of particulate matter may, after test- and material-specific adjustments, prove applicable also for micro- or nanoplastics studies.

Conclusions

The current study provides a rapid and accurate methodological approach for determining uptake and depuration kinetics by the single-celled freshwater organism, ciliated protozoa, of insoluble ENMs which are in the size range of phagocytosable particles (< 10 µm). The organism's physiology and feeding pattern facilitate optical microscopy image analysis and the conversion of the data to intracellular particle mass concentrations which allow quantitative measurements and expression of the results in the units conventionally used in bioaccumulation characterization. This permits the comparison of the uptake and depuration rates with the respective values determined in other studies and other organisms using different analytical methods. The use of a single-celled filter-feeding organism can also contribute to the efforts of reduction of animal use for *in vivo* testing if incorporated into tiered bioaccumulation testing[72] of insoluble particulate pollutants. Inter-individual variation in ENM uptake and depuration observed here in protozoa is a phenomenon that has been demonstrated also in the case of higher organisms such as fish, suggesting that ciliates may be employed as models for studying ecological impacts of the ingestion of ENMs or microplastics. Considering the widely reported high variation in ENM uptake rates across different species,[57, 58] the factors driving this variation warrant further investigation.

The method presented herein is mainly limited to insoluble larger (hydrodynamic diameter or at least one dimension > 100 nm)[28, 73] ENMs. This is due to measuring the food vacuole-confined ENMs and not the dissolved fraction of soluble metal-based ENMs or small ENMs which could potentially be taken up by alternative pathways to phagocytosis such as endocytosis through the cell membrane.[28, 32, 43, 74] Regardless, the image analysis-based method herein provides a verifiable means of quantifying uptake and depuration of carbon-based ENMs which otherwise significantly lack facile quantification methods.

Author Contributions

Monika Mortimer: Project administration, Methodology, Investigation, Formal analysis, Visualization, Writing – original draft, Writing – review & editing; Timnit Kefela: Investigation, Formal analysis, Visualization, Writing – original draft; Anne Trinh: Investigation, Formal analysis, Methodology; Patricia A. Holden: Conceptualization, Funding acquisition, Supervision, Writing – review & editing.

Conflicts of interest

There are no conflicts to declare.

Acknowledgements

This research was funded by the National Science Foundation (NSF) and the Environmental Protection Agency (EPA) under Cooperative Agreement DBI-0830117. Any opinions, findings, and conclusions expressed in this material are those of the authors and do not necessarily reflect those of either the NSF or EPA. This work was not subjected to EPA review, and no official endorsement should be inferred. T.K. acknowledges the scholarship of Robert L. Boughton Jr. through the University of California Santa Barbara (UCSB) Bren School of Environmental Science and Management and the Graduate Opportunity

Fellowship awarded by the UCSB Graduate Division. All authors acknowledge the use of the NRI-MCDB Microscopy Facility at UCSB.

References

1. M. S. Mauter, I. Zucker, F. Perreault, J. R. Werber, J.-H. Kim and M. Elimelech, The role of nanotechnology in tackling global water challenges, *Nat. Sustain.*, 2018, **1**, 166-175.
2. M. F. L. De Volder, S. H. Tawfick, R. H. Baughman and A. J. Hart, Carbon nanotubes: Present and future commercial applications, *Science*, 2013, **339**, 535-539.
3. P. A. Holden, F. Klaessig, R. F. Turco, J. H. Priester, C. M. Rico, H. Avila-Arias, M. Mortimer, K. Pacpaco and J. L. Gardea-Torresdey, Evaluation of exposure concentrations used in assessing manufactured nanomaterial environmental hazards: Are they relevant?, *Environ. Sci. Technol.*, 2014, **48**, 10541-10551.
4. A. Merlo, V. R. S. S. Mokkapati, S. Pandit and I. Mijakovic, Boron nitride nanomaterials: biocompatibility and bio-applications, *Biomater. Sci.*, 2018, **6**, 2298-2311.
5. M. Mortimer, N. Devarajan, D. Li and P. A. Holden, Multiwall carbon nanotubes induce more pronounced transcriptomic responses in *Pseudomonas aeruginosa* PG201 than graphene, exfoliated boron nitride, or carbon black, *ACS Nano*, 2018, **12**, 2728-2740.
6. M. Mortimer, D. Li, Y. Wang and P. A. Holden, Physical properties of carbon nanomaterials and nanoceria affect pathways important to the nodulation competitiveness of the symbiotic N_2 -fixing bacterium *Bradyrhizobium diazoefficiens*, *Small*, 2020, **16**, e1906055.
7. L. Dai, G. T. Banta, H. Selck and V. E. Forbes, Influence of copper oxide nanoparticle form and shape on toxicity and bioaccumulation in the deposit feeder, *Capitella teleta*, *Mar. Environ. Res.*, 2015, **111**, 99-106.
8. T. Ramskov, M.-N. Croteau, V. E. Forbes and H. Selck, Biokinetics of different-shaped copper oxide nanoparticles in the freshwater gastropod, *Potamopyrgus antipodarum*, *Aquat. Toxicol.*, 2015, **163**, 71-80.
9. A. Thit, A. Dybowska, C. Købler, G. Kennaway and H. Selck, Influence of copper oxide nanoparticle shape on bioaccumulation, cellular internalization and effects in the estuarine sediment-dwelling polychaete, *Nereis diversicolor*, *Mar. Environ. Res.*, 2015, **111**, 89-98.
10. N. W. van den Brink, A. J. Kokalj, P. V. Silva, E. Lahive, K. Norrfors, M. Baccaro, Z. Khodaparast, S. Loureiro, D. Drobne, G. Cornelis, S. Lofts, R. D. Handy, C. Svendsen, D. Spurgeon and C. A. M. van Gestel, Tools and rules for modelling uptake and bioaccumulation of nanomaterials in invertebrate organisms, *Environ. Sci. Nano*, 2019, **6**, 1985-2001.
11. A. Praetorius, N. Tufenkji, K.-U. Goss, M. Scheringer, F. von der Kammer and M. Elimelech, The road to nowhere: equilibrium partition coefficients for nanoparticles, *Environ. Sci. Nano*, 2014, **1**, 317-323.
12. E. J. Petersen, M. Mortimer, R. M. Burgess, R. Handy, S. Hanna, K. T. Ho, M. Johnson, S. Loureiro, H. Selck, J. J. Scott-Fordsmand, D. Spurgeon, J. Unrine, N. W. van den Brink, Y. Wang, J. White and P. Holden, Strategies for robust and accurate experimental approaches to quantify nanomaterial bioaccumulation across a broad range of organisms, *Environ. Sci. Nano*, 2019, **6**, 1619-1656.
13. S. Ouyang, X. Hu and Q. Zhou, Envelopment–Internalization Synergistic Effects and Metabolic Mechanisms of Graphene Oxide on Single-Cell *Chlorella vulgaris* Are Dependent on the Nanomaterial Particle Size, *ACS Appl. Mater. Interfaces*, 2015, **7**, 18104-18112.
14. M. Zhang, M. Yang, T. Morimoto, N. Tajima, K. Ichiraku, K. Fujita, S. Iijima, M. Yudasaka and T. Okazaki, Size-dependent cell uptake of carbon nanotubes by macrophages: A comparative and quantitative study, *Carbon*, 2018, **127**, 93-101.
15. D. G. Goodwin, A. S. Adeleye, L. Sung, K. T. Ho, R. M. Burgess and E. J. Petersen, Detection and Quantification of Graphene-Family Nanomaterials in the Environment, *Environ. Sci. Technol.*, 2018, **52**, 4491-4513.
16. E. J. Petersen, D. X. Flores-Cervantes, T. D. Bucheli, L. C. C. Elliott, J. A. Fagan, A. Gogos, S. Hanna, R. Kagi, E. Mansfield, A. R. M. Bustos, D. L. Plata, V. Reipa, P. Westerhoff and M. R. Winchester, Quantification of carbon nanotubes in environmental matrices: current capabilities, case studies, and future prospects, *Environ. Sci. Technol.*, 2016, **50**, 4587-4605.
17. R. Bjorkland, D. A. Tobias and E. J. Petersen, Increasing evidence indicates low bioaccumulation of carbon nanotubes, *Environ. Sci. Nano*, 2017, **4**, 747-766.
18. M. Mortimer, E. J. Petersen, B. A. Buchholz, E. Orias and P. A. Holden, Bioaccumulation of multiwall carbon nanotubes in *Tetrahymena thermophila* by direct feeding or trophic transfer, *Environ. Sci. Technol.*, 2016, **50**, 8876-8885.
19. S. Dong, T. Xia, Y. Yang, S. Lin and L. Mao, Bioaccumulation of 14C-Labeled Graphene in an Aquatic Food Chain through Direct Uptake or Trophic Transfer, *Environ. Sci. Technol.*, 2018, **52**, 541-549.
20. X. Cui, B. Wan, Y. Yang, X. Ren and L.-H. Guo, Length effects on the dynamic process of cellular uptake and exocytosis of single-walled carbon nanotubes in murine macrophage cells, *Sci. Rep.*, 2017, **7**, 1518.
21. R. C. Merrifield, C. Stephan and J. R. Lead, Quantification of Au Nanoparticle Biouptake and Distribution to Freshwater Algae Using Single Cell – ICP-MS, *Environ. Sci. Technol.*, 2018, **52**, 2271-2277.
22. Q. Wu, J. Shi, X. Ji, T. Xia, L. Zeng, G. Li, Y. Wang, J. Gao, L. Yao, J. Ma, X. Liu, N. Liu, L. Hu, B. He, Y. Liang, G. Qu and G. Jiang, Heterogenous Internalization of Nanoparticles at Ultra-Trace Concentration in Environmental Individual Unicellular Organisms Unveiled by Single-Cell Mass Cytometry, *ACS Nano*, 2020, **14**, 12828-12839.
23. L. Tong, Y. Liu, B. D. Dolash, Y. Jung, M. N. Slipchenko, D. E. Bergstrom and J.-X. Cheng, Label-free imaging of semiconducting and metallic carbon nanotubes in cells and mice using transient absorption microscopy, *Nat. Nanotechnol.*, 2012, **7**, 56-61.
24. J. K. Kim, J. H. Shin, J. S. Lee, J. H. Hwang, J. H. Lee, J. E. Baek, T. G. Kim, B. W. Kim, J. S. Kim, G. H. Lee, K. Ahn, S. G. Han, D. Bello and I. J. Yu, 28-Day inhalation toxicity of graphene nanoplatelets in Sprague-Dawley rats, *Nanotoxicology*, 2016, **10**, 891-901.
25. X. Hu, Y. Gao and Z. Fang, Integrating metabolic analysis with biological endpoints provides insight into nanotoxicological mechanisms of graphene oxide: From effect onset to cessation, *Carbon*, 2016, **109**, 65-73.

26. Y. Chen, X. Hu, J. Sun and Q. Zhou, Specific nanotoxicity of graphene oxide during zebrafish embryogenesis, *Nanotoxicology*, 2016, **10**, 42-52.
27. M. Mortimer, A. Gogos, N. Bartolome, A. Kahru, T. D. Bucheli and V. I. Slaveykova, Potential of hyperspectral imaging microscopy for semi-quantitative analysis of nanoparticle uptake by protozoa, *Environ. Sci. Technol.*, 2014, **48**, 8760-8767.
28. B. Huang, S. Yan, L. Xiao, R. Ji, L. Yang, A.-J. Miao and P. Wang, Label-Free Imaging of Nanoparticle Uptake Competition in Single Cells by Hyperspectral Stimulated Raman Scattering, *Small*, 2018, **14**, 1703246.
29. R. E. Mielke, J. H. Priester, R. A. Werlin, J. Gelb, A. M. Horst, E. Orias and P. A. Holden, Differential growth of and nanoscale TiO_2 accumulation in *Tetrahymena thermophila* by direct feeding versus trophic transfer from *Pseudomonas aeruginosa*, *Appl. Environ. Microbiol.*, 2013, **79**, 5616-5624.
30. Screening Assessment for the Challenge. Carbon Black, Environment Canada, Health Canada, 2013, 20-31.
31. Y. Wang, M. Mortimer, C. Chang and P. Holden, Alginic Acid-Aided Dispersion of Carbon Nanotubes, Graphene, and Boron Nitride Nanomaterials for Microbial Toxicity Testing, *Nanomaterials*, 2018, **8**, 76.
32. R. Werlin, J. H. Priester, R. E. Mielke, S. Kramer, S. Jackson, P. K. Stoimenov, G. D. Stucky, G. N. Cherr, E. Orias and P. A. Holden, Biomagnification of cadmium selenide quantum dots in a simple experimental microbial food chain, *Nat. Nanotechnol.*, 2011, **6**, 65-71.
33. V. Aruoja, S. Pokhrel, M. Sihtmae, M. Mortimer, L. Madler and A. Kahru, Toxicity of 12 metal-based nanoparticles to algae, bacteria and protozoa, *Environ. Sci.-Nano*, 2015, **2**, 630-644.
34. M. Mortimer, E. Petersen, B. Buchholz and P. Holden, Separation of Bacteria, Protozoa and Carbon Nanotubes by Density Gradient Centrifugation, *Nanomaterials*, 2016, **6**, 181.
35. WHO, The international pharmacopoeia [electronic resource] - 9th ed. Geneva: World Health Organization, 2019.
36. OECD, *Test No. 305: Bioaccumulation in Fish: Aqueous and Dietary Exposure*, 2012.
37. A. Karperien, ImageJ plugin Fraclac, https://imagej.nih.gov/ij/plugins/fraclac/FLHelp/Introduction.htm, accessed 2016).
38. M. Naito, T. Yokoyama, K. Hosokawa and K. Nogi, in *Nanoparticle Technology Handbook (Third Edition)*, eds. M. Naito, T. Yokoyama, K. Hosokawa and K. Nogi, Elsevier, 2018, DOI: 10.1016/B978-0-444-64110-6.00001-9, pp. 3-47.
39. N. Ibaseta and B. Biscans, Fractal dimension of fumed silica: Comparison of light scattering and electron microscope methods, *Powder Technol.*, 2010, **203**, 206-210.
40. R. J. Taylor, *An Introduction to Error Analysis*, University Science Books, Sausalito, California, USA, 1997.
41. Y. Ge, J. H. Priester, M. Mortimer, C. H. Chang, Z. Ji, J. P. Schimel and P. A. Holden, Long-term effects of multiwalled carbon nanotubes and graphene on microbial communities in dry soil, *Environ. Sci. Technol.*, 2016, **50**, 3965-3974.
42. G. B. Nanninga, A. Scott and A. Manica, Microplastic ingestion rates are phenotype-dependent in juvenile anemonefish, *Environ. Pollut.*, 2020, **259**, 113855.
43. M. Mortimer, A. Kahru and V. I. Slaveykova, Uptake, localization and clearance of quantum dots in ciliated protozoa *Tetrahymena thermophila*, *Environ. Pollut.*, 2014, **190**, 58-64.
44. M. Mortimer, K. Kasemets, M. Vodovnik, R. Marinsek-Logar and A. Kahru, Exposure to CuO nanoparticles changes the fatty acid composition of protozoa *Tetrahymena thermophila*, *Environ. Sci. Technol.*, 2011, **45**, 6617-6624.
45. M. W. Hahn and M. G. Höfle, Grazing of protozoa and its effect on populations of aquatic bacteria, *FEMS Microbiol. Ecol.*, 2001, **35**, 113-121.
46. American Elements, https://www.americanelements.com/carbon-black-nanoparticles-nanopowder-1333-86-4, (accessed October 6, 2021).
47. Orion Engineered Carbons, http://www.matweb.com/search/datasheet_print.aspx?matguid=fbe06bc098204beb894a6f87af05fa30, (accessed October 6, 2021).
48. M. J. Wang, Gray, C.A., Reznek, S.A., Mahmud, K. and Kutsovsky, Y., in *Kirk-Othmer Encyclopedia of Chemical Technology*, Wiley, 2003, DOI: https://doi.org/10.1002/0471238961.0301180204011414.a01.pub2.
49. US Research Nanomaterials, Inc, https://www.us-nano.com/inc/sdetail/28840, (accessed October 6, 2021).
50. Avansa Technology & Services, http://www.avansa.co.in/carbon-nanotube.html, (accessed October 6, 2021).
51. CheapTubes Inc., https://www.cheaptubes.com/product/multi-walled-carbon-nanotubes-30-50nm/, (accessed November 15, 2020).
52. Strem Chemicals, Inc, https://www.strem.com/uploads/resources/documents/graphene_nanoplatelets_copy1.pdf, (accessed October 6, 2021).
53. E. Pop, V. Varshney and A. K. Roy, Thermal properties of graphene: Fundamentals and applications, *MRS Bulletin*, 2012, **37**, 1273-1281.
54. J. Greim and K. A. Schwetz, in *Ullmann's Encyclopedia of Industrial Chemistry*, 2006, DOI: https://doi.org/10.1002/14356007.a04_295.pub2.
55. J. R. Nilsson, On Food Vacuoles in *Tetrahymena pyriformis* GL, *J. Protozool.*, 1977, **24**, 502-507.
56. H. M. Maes, F. Stibany, S. Giefers, B. Daniels, B. Deutschmann, W. Baumgartner and A. Schaffer, Accumulation and distribution of multiwalled carbon nanotubes in zebrafish (*Danio rerio*), *Environ. Sci. Technol.*, 2014, **48**, 12256-12264.
57. S. Rhiem, M. J. Riding, W. Baumgartner, F. L. Martin, K. T. Semple, K. C. Jones, A. Schaffer and H. M. Maes, Interactions of multiwalled carbon nanotubes with algal cells: Quantification of association, visualization of uptake, and measurement of alterations in the composition of cells, *Environ. Pollut.*, 2015, **196**, 431-439.
58. C. W. Isaacson, L. Sigg, A. A. Ammann, J. Stadnicka-Michalak and K. Schirmer, Interactions of TiO_2 nanoparticles and the freshwater nematode *Plectus aquatilis*: particle properties, kinetic parameters and bioconcentration factors, *Environ. Sci. Nano*, 2017, **4**, 712-719.

59. L. Mao, C. Liu, K. Lu, Y. Su, C. Gu, Q. Huang and E. J. Petersen, Exposure of few layer graphene to *Limnodrilus hoffmeisteri* modifies the graphene and changes its bioaccumulation by other organisms, *Carbon*, 2016, **109**, 566-574.
60. X. Guo, S. Dong, E. J. Petersen, S. Gao, Q. Huang and L. Mao, Biological Uptake and Depuration of Radio-labeled Graphene by *Daphnia magna*, *Environ. Sci. Technol.*, 2013, **47**, 12524-12531.
61. E. J. Petersen, J. Akkanen, J. V. K. Kukkonen and W. J. Weber, Jr., Biological uptake and depuration of carbon nano-tubes by *Daphnia magna*, *Environ. Sci. Technol.*, 2009, **43**, 2969-2975.
62. K. Lu, S. Dong, E. J. Petersen, J. Niu, X. Chang, P. Wang, S. Lin, S. Gao and L. Mao, Biological Uptake, Distribution, and Depuration of Radio-Labeled Graphene in Adult Zebrafish: Effects of Graphene Size and Natural Organic Matter, *ACS Nano*, 2017, **11**, 2872-2885.
63. J. A. Arnot and F. A. P. C. Gobas, A review of bioconcentration factor (BCF) and bioaccumulation factor (BAF) assessments for organic chemicals in aquatic organisms, *Environ. Rev.*, 2006, **14**, 257-297.
64. E. J. Petersen, R. A. Pinto, D. J. Mai, P. F. Landrum and W. J. Weber, Influence of polyethyleneimine graftings of multi-walled carbon nanotubes on their accumulation and elimination by and toxicity to *Daphnia magna*, *Environ. Sci. Technol.*, 2011, **45**, 1133-1138.
65. M.-K. Yeo and D.-H. Nam, Influence of different types of nanomaterials on their bioaccumulation in a paddy microcosm: A comparison of TiO_2 nanoparticles and nanotubes, *Environ. Pollut.*, 2013, **178**, 166-172.
66. T. Gouin, Toward an Improved Understanding of the Ingestion and Trophic Transfer of Microplastic Particles: Critical Review and Implications for Future Research, *Environ. Toxicol. Chem.*, 2020, **39**, 1119-1137.
67. M. Ogonowski, C. Schür, Å. Jarsén and E. Gorokhova, The Effects of Natural and Anthropogenic Microparticles on Individual Fitness in *Daphnia magna*, *PLOS ONE*, 2016, **11**, e0155063.
68. B. Fernández and M. Albentosa, Insights into the uptake, elimination and accumulation of microplastics in mussel, *Environ. Pollut.*, 2019, **249**, 321-329.
69. S. Y. Au, T. F. Bruce, W. C. Bridges and S. J. Klaine, Responses of *Hyalella azteca* to acute and chronic microplastic exposures, *Environ. Toxicol. Chem.*, 2015, **34**, 2564-2572.
70. R. R. Hurley, J. C. Woodward and J. J. Rothwell, Ingestion of Microplastics by Freshwater Tubifex Worms, *Environ. Sci. Technol.*, 2017, **51**, 12844-12851.
71. R. Qiao, Y. Deng, S. Zhang, M. B. Wolosker, Q. Zhu, H. Ren and Y. Zhang, Accumulation of different shapes of microplastics initiates intestinal injury and gut microbiota dysbiosis in the gut of zebrafish, *Chemosphere*, 2019, **236**, 124334.
72. R. D. Handy, J. Ahtiainen, J. M. Navas, G. Goss, E. A. J. Bleeker and F. von der Kammer, Proposal for a tiered dietary bioaccumulation testing strategy for engineered nanomaterials using fish, *Environ. Sci. Nano*, 2018, **5**, 2030-2046.
73. L. Rasmussen, Nutrient uptake in *Tetrahymena pyriformis*, *Carlsberg Res. Commun.*, 1976, **41**, 143-167.
74. C. Wu, W.-B. Guo, Y.-Y. Liu, L. Yang and A.-J. Miao, Molecular mechanisms underlying the calcium-mediated uptake of hematite nanoparticles by the ciliate *Tetrahymena thermophila*, *Environ. Pollut.*, 2021, **288**, 117749.